Baku State University Journal of Chemistry and Material Sciences, 2025, v. 2 (2), p.1-9

journal homepage: *http://bsuj.bsu.edu.az/en*
https://doi.org/10.30546/209501.201.2025.2.02.09

SURFACE-ENGINEERED Fe_3O_4 NANOPARTICLES FOR ENHANCED ANTICANCER DRUG LOADING

Aynura Karimova, Aygun Mehdiyeva, Sevinj Nuriyeva, Habiba Shirinova, Lala Gahramanli
Baku State University, Baku, Azerbaijan

Received: 10 March 2025
Accepted: 28 April 2025
Published: 24 June 2025

This study focuses on the synthesis, surface modification, and drug loading of iron oxide (Fe_3O_4) nanoparticles for potential cancer therapy. Fe_3O_4 nanoparticles were synthesized using a co-precipitation method, followed by surface coating with dextran and cross-linked dextran. The model anticancer drug, 5,7-dihydroxyflavone, was loaded onto the nanoparticles using physical adsorption. The structural characteristics of the prepared samples were analyzed using Fourier-transform infrared (FTIR) and ultraviolet-visible (UV-Vis) spectroscopy. FTIR analysis confirmed successful surface functionalization, while the drug loading efficiency was quantified by UV-Vis. spectroscopy. Mathematical calculations based on UV-Vis. absorbance data showed that the 5,7-dihydroxyflavone loading efficiency of Fe_3O_4/CL-Dex/Drug (~43%) was approximately 7% higher than that of Fe_3O_4/Dex/Drug (~36%). These results demonstrate that cross-linked dextran significantly improved the stability and drug-loading capacity of the nanoparticles. The enhanced drug loading efficiency further supports the hypothesis that Fe_3O_4/CL-Dex/Drug nanoparticles are more effective nanocarrier system for hydrophobic bioactive compounds.

This study highlights the importance of surface modification in enhancing the stability and efficacy of Fe_3O_4 nanoparticles for biomedical applications, particularly in targeted drug delivery for cancer treatment.

Keywords: iron oxide nanoparticles, dextran, cross-linked dextran, anticancer drug, surface coating, drug loading efficiency, drug delivery

INTRODUCTION

In recent years, iron oxide nanoparticles have garnered significant attention for their promising applications in biomedical engineering, medicine, and related disciplines [1, 2]. One of the primary reasons for their broad applicability is their unique magnetic properties. When synthesized at ultra-small sizes - typically between 10–30 nm - ferromagnetic crystals, for instance, magnetite Fe_3O_4 nanoparticles can exhibit superparamagnetism [3]. In this state, electron spins within each nanoparticle align collectively, and the particle behaves as a single magnetic domain. A key advantage of superparamagnetic nanoparticles over other magnetic forms lies in their high magnetization under an external magnetic field, which diminishes to near zero once the field is removed. This reversible behavior makes iron oxide nanoparticles particularly suitable for biomedical use.

Superparamagnetic iron oxide nanoparticles have been successfully employed in a wide range of applications including biosensors, magnetic resonance imaging (MRI), magnetic hyperthermia, and targeted drug delivery systems [4, 5, 6, 7]. Among these, magnetically-guided drug delivery is a therapeutic strategy designed to minimize systemic side effects by

E-mail address: aynurakarimova@bsu.edu.az

directing therapeutic agents specifically to diseased tissues. In such systems, drugs are loaded onto magnetic nanoparticles and guided to the target site under the influence of an external magnetic field [7]. This approach has shown particular effectiveness in cancer therapy, allowing for the reduction of drug dosage and frequency in chemotherapy patients.

Iron oxide-based magnetic nanoparticles are ideal candidates for biomedical applications due to their high saturation magnetization and the ability to control their movement and localization via magnetic fields. However, these nanoparticles exhibit increased surface energy at the nanoscale, which promotes particle aggregation and growth [8]. To prevent this instability and enhance biocompatibility, surface modification is employed using naturally derived, biocompatible polymers [9]. Such coatings improve particle stability, prevent aggregation, and can enhance target specificity in biological environments. Commonly used surface modifiers include dextran [10], polyethylene glycol (PEG) [11], chitosan [12], collagen [13], alginate [14], etc.

In study [15], chitosan-coated iron oxide nanoparticles were synthesized and evaluated for their potential to enhance bone regeneration at defect sites. The synthesis involved co-precipitation of 5 mL iron (III) chloride (0.25 M) and 5 mL iron (II) sulfate in aqueous solution. The mixture was stirred under nitrogen at 45°C for 20 minutes to eliminate dissolved oxygen, followed by the addition of 40 mL ammonium hydroxide. Stirring continued for another 30 minutes, resulting in nanoparticles precipitation. The product was washed 4 times with distilled water and then modified by adding 0.2 mg/mL chitosan under constant agitation. The resulting chitosan-coated iron oxide nanoparticles were characterized using transmission electron microscopy (TEM), dynamic light scattering (DLS), X-ray diffraction (XRD), and zeta potential analysis. Cellular uptake by osteoblasts was examined via TEM and Prussian blue staining. Results demonstrated that chitosan coating enhanced osteoblast proliferation while minimizing damage to the cell membrane.

Another study [16] involved a two-step synthesis process to produce PEG-coated iron oxide nanoparticles using co-precipitation followed by surface modification. PEG-coated iron oxide nanoparticles are of interest due to their use in MRI, magnetic hyperthermia, and drug delivery. Various concentrations of PEG were tested to examine its impact on particle structure and magnetic properties. Characterization was performed using XRD, FTIR spectroscopy, and TEM. The average nanoparticle size remained consistent (7-8 nm) despite increasing PEG concentrations. Thermogravimetric analysis showed that PEG coverage increased from 2.6% to 6.9% as PEG mass increased from 5 g to 15 g. Notably, PEG-coated iron oxide nanoparticles exhibited higher saturation magnetization (M_s) than uncoated counterparts, reaching 62.4 emu/g, while preserving superparamagnetic behavior. These findings indicate that PEG improves magnetic tunability and enhances the nanoparticles' suitability for biomedical applications.

In summary, the performance and applicability of iron oxide nanoparticles are strongly influenced by surface engineering strategies. For the successful implementation of targeted drug delivery systems, a comprehensive understanding of the physicochemical properties of the nanocarriers is essential. In this context, the current study focuses on the chemical synthesis of iron oxide nanoparticles, their surface coating with dextran and cross-linked dextran, loading with anticancer drugs, and a comparative analysis of their structural characteristics and performance.

EXPERIMENTAL

Materials and Methods

Ferric chloride hexahydrate ($FeCl_3 \cdot 6H_2O$, 98%), ferrous sulfate heptahydrate ($FeSO_4 \cdot 7H_2O$, 98%), and ammonium hydroxide solution (NH_4OH, 23-25%) were utilized for the preparation of Fe_3O_4 nanoparticles. Dextran ($(C_6H_{10}O_5)_n$, molecular weight ~40,000) served as the surface stabilizer. Glutaraldehyde (GA, $C_5H_8O_2$, 25%) acted as a crosslinking agent. 5,7-dihydroxyflavone ($C_{15}H_{10}O_4$, 99,93%) was selected as the model anticancer compound, while N, N-dimethylformamide (DMF, C_3H_7NO, 99.8%) was employed as the solvent. All reagents were used as received without additional purification.

Preparation of Coated Iron Oxide Nanoparticles

Fe_3O_4 nanoparticles were synthesized using a co-precipitation method as outlined in earlier studies [17]. In brief, a homogeneous aqueous solution containing $FeCl_3 \cdot 6H_2O$ and $FeSO_4 \cdot 7H_2O$ in a 2:1 molar ratio was prepared in 50 mL of deionized water and stirred at 400 rpm. The mixture was then heated to 70 °C for 30 minutes under a nitrogen atmosphere to remove dissolved oxygen and prevent the oxidation of Fe_3O_4 to γ-Fe_2O_3. To stabilize the nanoparticles, dextran was gradually introduced into the solution while stirring continued for approximately 1 hour.

Subsequently, 10-15 mL of 23-25% NH_4OH solution was added dropwise. A black precipitate formed immediately upon addition, indicating nanoparticle formation. The overall reaction can be summarized as:

$$Fe^{2+} + 2Fe^{3+} + 8OH^- \rightarrow Fe(OH)_2 + 2Fe(OH)_3 \rightarrow Fe_3O_4\downarrow + 4H_2O \quad (1)$$

To regulate particle size, both pH and temperature were closely monitored throughout the synthesis [18]. The reaction was allowed to proceed for an additional hour under continuous stirring. The final pH reached approximately 10-11.

After completion, the reaction mixture was placed near a neodymium magnet (NdFeB) to separate the Fe_3O_4 nanoparticles. The supernatant was decanted, and the residue was washed repeatedly with deionized water until neutral pH was achieved. The resulting dextran-coated Fe_3O_4 (Fe_3O_4/Dex) nanoparticles were then dried at 60°C for 4 hours in an oven.

To obtain crosslinked dextran-coated Fe_3O_4 nanoparticles (Fe_3O_4/CL-Dex), glutaraldehyde (GA) was added during the nanoparticle formation process. The mixture was stirred for an additional hour to promote crosslinking. The subsequent washing and drying procedures were identical to those used for the non-crosslinked nanoparticles.

Loading of Drug

The loading of 5,7-dihydroxyflavone into the Fe_3O_4/Dex NPs was realized using the physical adsorption method. Briefly, drug was solubilized in DMF, and was subsequently added to the Fe_3O_4/Dex powder. Then the mixture was stirred with a mechanical stirrer at 500 rpm for 5-6 hours at room temperature. Following the procedure, the drug loaded nanoparticles (Fe_3O_4/Dex/Drug) were isolated from the solution by centrifuging at 10.000 rpm. In order to eliminate weakly adsorbed drugs on the surface, they were washed with deionized water. Next, 5,7-dihydroxyflavone loaded samples were dried in an oven at 60°C for 4 hours. The synthesis of crosslinked dextran-coated and drug-loaded iron oxide nanoparticles (Fe_3O_4/CL-Dex/Drug) followed the same protocol.

Characterization Techniques

The structural and chemical properties, along with the drug-loading efficiency of the samples, were assessed using Fourier-transform infrared (FTIR) and ultraviolet-visible (UV-Vis.) spectroscopy. The molecular structure was analyzed using a Varian 3600 FTIR spectrometer with KBr pellets, capturing the spectrum in the range of 4000–500 cm^{-1}. The drug-loading efficiency for all samples was evaluated using a Specord250 PLUS UV-Vis. spectrometer.

Drug-Loading Efficiency

The loading efficiency of 5,7-dihydroxyflavone onto Fe_3O_4/Dex and Fe_3O_4/CL-Dex nanoparticles was determined by analyzing the concentration of unbound drug in the supernatant following nanoparticle - drug incubation and centrifugation. The samples suspensions were centrifuged at 10.000 rpm for 5 minutes, and the supernatant was collected for analysis. The concentration of unloaded drug was measured using UV-Vis. spectroscopy at a wavelength of 276.4 nm. The loading efficiency was then determined by subtracting the amount of free 5,7-dihydroxyflavone (D_{free}) from the initial total amount of drug added (D_{total}) and expressing the result as a percentage of the total. The following formula was used [17]:

$$Loading\ efficiency = \frac{(D_{total} - D_{free})}{D_{total}} \times 100\% \quad (2)$$

RESULTS AND DISCUSSION

The absorption spectra of the synthesized samples were analyzed using the FTIR method in the range of 4000 - 500 cm^{-1}. Figure 1 presents the FTIR spectra of the Fe_3O_4/Dex and Fe_3O_4/CL-Dex samples.

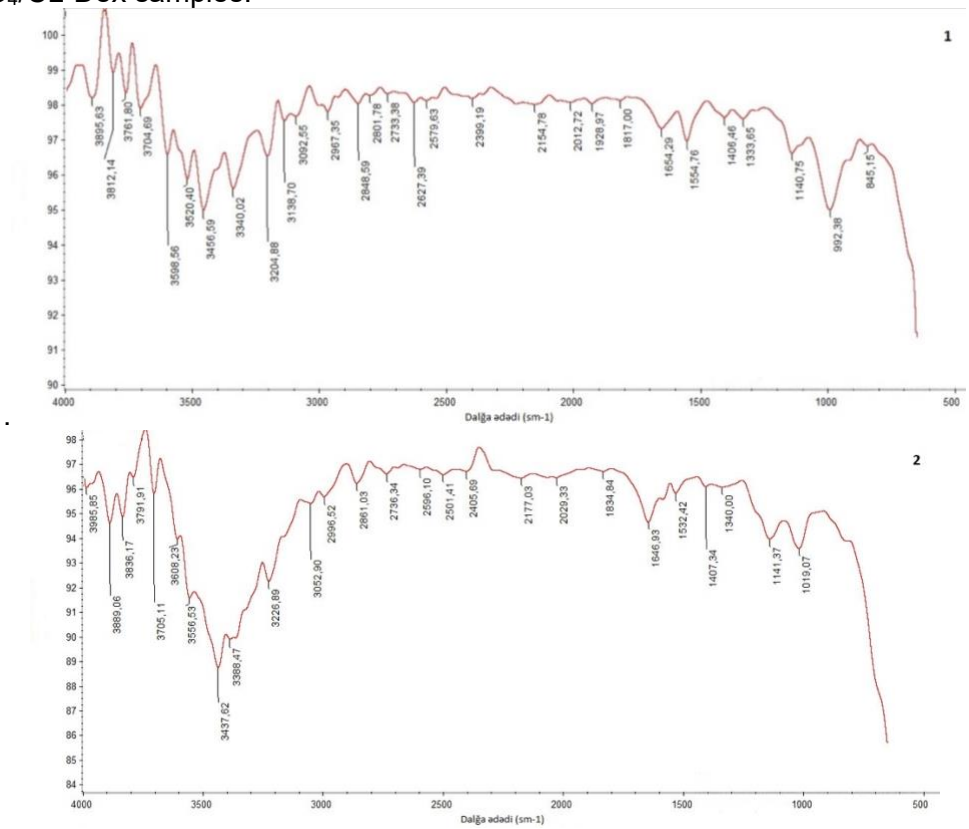

Figure 1. FTIR spectra of Fe_3O_4/Dex (1) and Fe_3O_4/CL-Dex (2) samples

In the FTIR spectrum of the Fe_3O_4/Dex sample, the band observed at 1140 cm^{-1} is attributed to the covalent vibrations of the glycosidic linkage. In the Fe_3O_4/CL-Dex sample, this band remains at a similar position (1141 cm^{-1}), indicating that dextran is still present in the system following the crosslinking process. The band at 992 cm^{-1} in the Fe_3O_4/Dex sample corresponds to the C-O stretching vibration associated with the fourth carbon of the glucose residue. In the Fe_3O_4/CL-Dex sample, this band shifts to 1019 cm^{-1}, which may be indicative of modifications in the glycosidic linkage structure as a result of crosslinking.

The broad absorption bands observed in the range of approximately 3000-3600 cm^{-1} in both samples are characteristic of the O-H stretching vibrations of hydroxyl groups present in the polysaccharide matrix [19]. In the Fe_3O_4/CL-Dex sample, noticeable shifts and intensity changes within this range, compared to the Fe_3O_4/Dex sample, suggest a reduction in hydroxyl content and structural alterations due to the crosslinking process.

Both samples display absorption bands in the region of ~2800-2900 cm^{-1}, which are attributed to symmetric and asymmetric stretching vibrations of C-H bonds in methyl groups. Additionally, the appearance of bands at 1646 and 1532 cm^{-1} in the Fe_3O_4/CL-Dex sample is associated with the formation of imine (C=N) bonds, indicating successful crosslinking of dextran chains via glutaraldehyde [20].

Changes observed in the 800–900 cm^{-1} region are attributed to the bending vibrations of the α-glucopyranose ring, reflecting modifications in the organic structure of dextran [21].

The presence of these vibrational modes confirms the effective surface functionalization of the iron oxide nanoparticles.

Figure 2 presents the FTIR spectra of the drug-loaded and dextran-coated iron oxide nanoparticles.

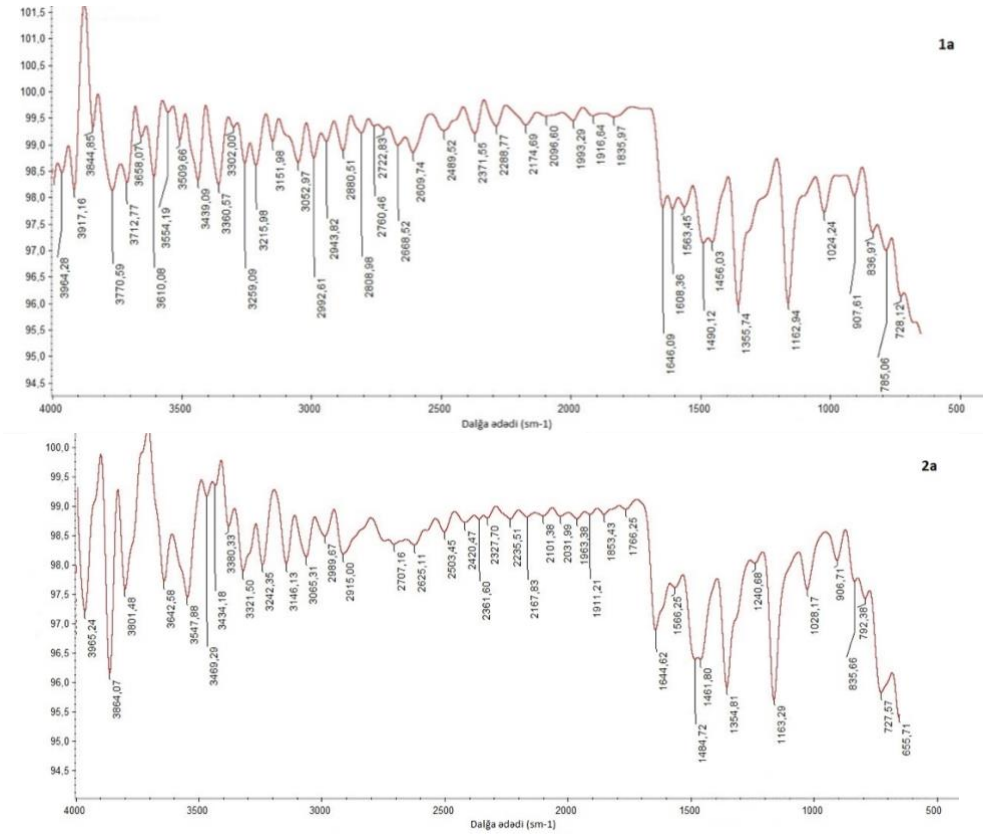

Figure 2. FTIR spectra of Fe_3O_4/Dex/Drug (1a) and Fe_3O_4/CL-Dex/Drug (2a) samples

The spectra of both samples differ significantly from those of the non-drug-loaded Fe_3O_4 nanoparticles (Figure 1). The most notable differences were observed in the region associated with the stretching vibrations of -OH groups (~3000-3600 cm^{-1}). This indicates the formation of hydrogen bonds between the drug and the coating materials in both samples [22]. In the Fe_3O_4/CL-Dex/Drug sample, the bands in this region shifted toward lower wavenumbers and showed higher intensity compared to the Fe_3O_4/Dex/Drug sample. This can be attributed to the conformational changes in the dextran molecules following crosslinking, which facilitate stronger hydrogen bonding interactions between the -OH groups and the drug. Stronger hydrogen bonding results in vibrational transitions at lower energy (lower wavenumber) and generates more intense signals.

In the Fe_3O_4/Dex/Drug sample, new peaks at 1563 and 1490 cm^{-1} correspond to the C-C stretching vibrations in the aromatic ring of 5,7-dihydroxyflavone [23]. These same peaks, with slight shifts (at 1566 and 1485 cm^{-1}, respectively), were also observed in the Fe_3O_4/CL-Dex/Drug sample. The bands at 1456 cm^{-1} and 1461 cm^{-1} in the Fe_3O_4/Dex/Drug and Fe_3O_4/CL-Dex/Drug samples, respectively, are attributed to the C-O-H vibrations of the aromatic ring in chrysin [24]. Additionally, both drug-loaded samples exhibited a band around 1024 cm^{-1} corresponding to the C-O-C stretching vibrations in the central heterocyclic ring of chrysin [25].

Furthermore, new bands appeared in the Fe_3O_4/Dex/Drug sample compared to Fe_3O_4/Dex in the 700–900 cm^{-1} range. Specifically, the bands at 785, 836, and 907 cm^{-1} are associated with out-of-plane bending vibrations of C-H groups in the aromatic ring of 5,7-dihydroxyflavone [26]. In the Fe_3O_4/CL-Dex/Drug sample, these peaks retained their positions, except for the 785 cm^{-1} band, which shifted slightly to 792 cm^{-1}. This shift may be due to the

formation of a denser and more rigid environment around the nanoparticles following crosslinking, leading to stronger interactions with the drug. The presence of these characteristic bands related to 5,7-dihydroxyflavone in both Fe_3O_4/Dex/Drug and Fe_3O_4/CL-Dex/Drug samples confirms that the chemical structure of the drug was preserved and was successfully loaded onto the nanosystem via physical interaction.

Thus, based on FTIR analysis, it was determined that drug was successfully loaded onto the surface coated Fe_3O_4 nanoparticles. The Fe_3O_4/CL-Dex/Drug sample exhibited a stronger interaction with 5,7-dihydroxyflavone, compared to Fe_3O_4/Dex/Drug nanoparticles, which can be explained by the formation of additional hydrogen bonds.

In the study, the effectiveness of the loading efficiency of the obtained samples as a potential nanocarrier tool for 5,7-dihydroxyflavone was spectrophotometrically analyzed at 276.4 nm [27]. Table 1 shows the drug loading efficiency for samples obtained with various coating strategies.

Table 1. Mathematically calculated loading efficiency results of 5,7-dihydroxyflavone for the samples

Samples	Loading efficiency (%)
Fe_3O_4/Dex/Drug	36
Fe_3O_4/CL-Dex/Drug	43

Thus, based on the UV-Vis. spectral results of the samples, the successful loading of 5,7-dihydroxyflavone onto polymer coated iron oxide nanoparticles was confirmed. Compared to dextran-coated samples, the use of crosslinked dextran as a coating material led to an approximately 7% increase in drug loading efficiency.

CONCLUSION

The successful loading of the drug onto polymer coated Fe_3O_4 nanoparticles was confirmed through both FTIR and UV-Vis. spectroscopic analyses. Characteristic vibrational bands corresponding to the aromatic groups of 5,7-dihydroxyflavone were clearly observed in the FTIR spectra of Fe_3O_4/Dex/Drug and Fe_3O_4/CL-Dex/Drug, indicating effective drug incorporation into the nanocarrier systems. Furthermore, FTIR results revealed stronger intermolecular interactions between the drug and the Fe_3O_4/CL-Dex/Drug nanoparticles compared to the non-crosslinked dextran-coated counterpart. This can be attributed to the formation of additional hydrogen bonds due to the higher density of functional groups provided by the crosslinked dextran.

Mathematical calculations based on UV-Vis. absorbance data showed that the 5,7-dihydroxyflavone loading efficiency of Fe_3O_4/CL-Dex/Drug (~43%) was approximately 7% higher than that of Fe_3O_4/Dex/Drug (~36%). This enhancement further supports the hypothesis that crosslinked dextran provides a more stable and favorable structural environment for drug adsorption, making Fe_3O_4/CL-Dex/Drug a more effective nanocarrier system for hydrophobic bioactive compounds.

REFERENCES

[1] Arias, L.S.; Pessan, J.P.; Vieira, A.P.M.; Lima, T.M.T.; Delbem, A.C.B.; Monteiro, D.R. Iron Oxide Nanoparticles for Biomedical Applications: A Perspective on Synthesis, Drugs, Antimicrobial Activity, and Toxicity, *Antibiotics (Basel),* **2018**, 7(2), pp. 1–16, https://doi.org/10.3390/antibiotics7020046

[2] Attia, N.F.; Abd El-Monaem, E.M.; El-Aqapa, H.G.; Elashery, S.E.A.; Eltaweil, A.S.; El Kady, M.; Khalifa, S.A.M.; Hawash, H.B.; El-Seedi, H.R. Iron Oxide Nanoparticles and

Their Pharmaceutical Applications, *Applied Surface Science Advances,* **2022**, **11**, 100284, https://doi.org/10.1016/j.apsadv.2022.100284

[3] Cruz, M.M.; Ferreira, L.P.; Alves, A.F.; Mendo, S.G.; Ferreira, P.; Godinho, M.; Carvalho, M.D. Chapter 19 – Nanoparticles for Magnetic Hyperthermia, in: Ficai, A.; Grumezescu, A.M. (Eds.), *Nanostructures for Cancer Therapy*, *Micro and Nano Technologies*, Elsevier, **2017**, pp. 485–511, https://doi.org/10.1016/B978-0-323-46144-3.00019-2

[4] Hanoglu, S.B.; Harmanci, D.; Ucar, N.; Evran, S.; Timur, S. Recent Approaches in Magnetic Nanoparticle-Based Biosensors of miRNA Detection, *Magnetochemistry,* **2023**, 9(1), 23, pp. 1-25, https://doi.org/10.3390/magnetochemistry9010023

[5] Jin, R.; Lin, B.; Li, D.; Ai, H. Superparamagnetic Iron Oxide Nanoparticles for MR Imaging and Therapy: Design Considerations and Clinical Applications, *Current Opinion in Pharmacology*, **2014**, 18, pp. 18–27, https://doi.org/10.1016/j.coph.2014.08.002

[6] Pucci, C.; Degl'Innocenti, A.; Belenli Gümüş, M.; Ciofani, G. Superparamagnetic Iron Oxide Nanoparticles for Magnetic Hyperthermia: Recent Advancements, Molecular Effects, and Future Directions in the Omics Era, *Biomaterials Science*, **2022**, 10(9), pp. 2103–2121, https://doi.org/10.1039/d1bm01963e

[7] Ramazanov, M.; Karimova, A.; Shirinova, H. Magnetism for Drug Delivery, MRI and Hyperthermia Applications: A Review, *Biointerface Research in Applied Chemistry,* **2021**, 11(2), pp. 8654–8668, https://doi.org/10.33263/BRIAC112.86548668

[8] Stiufiuc, G.F.; Stiufiuc, R.I. Magnetic Nanoparticles: Synthesis, Characterization, and Their Use in Biomedical Field, *Applied Sciences*, **2024**, 14(4), pp. 1623-1651, https://doi.org/10.3390/app14041623

[9] Zhu, N.; Ji, H.; Yu, P.; Niu, J.; Farooq, M.U.; Akram, M.W.; Udego, I.O.; Li, H.; Niu, X. Surface Modification of Magnetic Iron Oxide Nanoparticles, *Nanomaterials*, **2018**, 8(10), pp. 810-837, https://doi.org/10.3390/nano8100810

[10] Hong, R.R.; Feng, B.; Chen, L.L.; Wei, D.; Li, H.; Zhai, G.; Liu, J.; Yang, F. Synthesis, Characterization and MRI Application of Dextran-Coated Fe_3O_4 Magnetic Nanoparticles, *Biochemical Engineering Journal*, **2008**, 42(3), pp. 290–300, https://doi.org/10.1016/j.bej.2008.07.009

[11] Mannu, R.; Karthikeyan, V.; Velu, N.; Arumugam, C.; Roy, V.A.L.; Gopalan, A.I.; Saianand, G.; Sonar, P.; Lee, K.P.; Kim, W.J.; Lee, D.E.; Kannan, V. Polyethylene Glycol Coated Magnetic Nanoparticles: Hybrid Nanofluid Formulation, Properties and Drug Delivery Prospects, *Nanomaterials*, **2021**, 11(2), pp. 440-458, https://doi.org/10.3390/nano11020440

[12] Albutt, N.; Sonsupap, S.; Sinprachim, T.; Thonglor, P. Synthesis of Magnetic Nanoparticles Coated with Chitosan for Biomedical Applications, *Key Engineering Materials*, **2024**, 1005, pp. 49-57, https://doi.org/10.4028/p-9xdPMD

[13] Sande, M.G.; Roque, L.; Braga, A.; Marques, M.; Ferreira, D.; Saragliadis, A.; Rodrigues, J.L.; Linke, D.; Ramada, D.; Silva, C.; Rodrigues, L.R. Design of New Hydrolyzed Collagen-Modified Magnetic Nanoparticles to Capture Pathogens, *Journal of Biomedical Materials Research Part B: Applied Biomaterials*, **2023**, 111(2), pp. 354-365, https://doi.org/10.1002/jbm.b.35155

[14] Kloster, G.A.; Muraca, D.; Moscoso Londoño, O.; Pirota, K.R.; Mosiewicki, M.A.; Marcovich, N.E. Alginate-Based Nanocomposites with Magnetic Properties, *Composites Part A: Applied Science and Manufacturing*, **2020**, 135, 105936, pp. 1-11, https://doi.org/10.1016/j.compositesa.2020.105936

[15] Gómez Pérez, A.; González-Martínez, E.; Díaz Águila, C.R.; González-Martínez, D.A.; González Ruiz, G.; García Artalejo, A.; Yee-Madeira, H. Chitosan-Coated Magnetic Iron Oxide Nanoparticles for DNA and rhEGF Separation, *Colloids and Surfaces A: Physicochemical and Engineering Aspects*, **2020**, 591, 124500, pp. 1-27, https://doi.org/10.1016/j.colsurfa.2020.124500

[16] Karaagac, O.; Köçkar, H. Improvement of the Saturation Magnetization of PEG Coated Superparamagnetic Iron Oxide Nanoparticles, *Journal of Magnetism and Magnetic Materials*, **2022**, 551, 169140, pp. 1-8, https://doi.org/10.1016/j.jmmm.2022.169140

[17] Karimova, A.; Hajizada, S.; Shirinova, H.; Nuriyeva, S.; Gahramanli, L.; Yusuf, M.M.; Bellucci, S.; Reissfelder, C.; Yagublu, V. Surface Modification Strategies for Chrysin-Loaded Iron Oxide Nanoparticles to Boost Their Anti-Tumor Efficacy in Human Colon Carcinoma Cells, *J. Funct. Biomater.*, **2024**, 15, 43, pp. 1-14, https://doi.org/10.3390/jfb15020043

[18] Dudchenko, N.; Pawar, S.; Perelshtein, I.; Fixler, D. Magnetite Nanoparticles: Synthesis and Applications in Optics and Nanophotonics, *Materials,* **2022**, 15, 2601, pp. 1–20, https://doi.org/10.3390/ma15072601

[19] Ra'ad, Z.; Al-Karam, L.; Al-Karam, L.; Abid Alsahib, N. K. Synthesis and Characterization of Dextran Coated Iron Oxide Nanoparticles as a T1 Contrast Agent, *Journal of Physics: Conference Series*, **2021**, 2114, 012037, pp. 1-8, https://doi.org/10.1088/1742-6596/2114/1/012037

[20] Hoffmann, B.; Seitz, D.; Mencke, A.; Kokott, A.; Ziegler, G. Glutaraldehyde and Oxidised Dextran as Crosslinker Reagents for Chitosan-Based Scaffolds for Cartilage Tissue Engineering, *Journal of Materials Science: Materials in Medicine*, **2009**, 20, pp. 1495-1503, https://doi.org/10.1007/s10856-009-3707-3

[21] Nikonenko, N. A.; Buslov, D. K.; Sushko, N. I.; Zhbankov, R. G. Investigation of Stretching Vibrations of Glycosidic Linkages in Disaccharides and Polysaccharides with Use of IR Spectra Deconvolution, *Peptide Science*, **2000**, 57(4), pp. 257-262, https://doi.org/10.1002/1097-0282(2000)57:4<257::AID-BIP7>3.0.CO;2-3

[22] Glišić, S.; Nikolić, G. S.; Cakić, M. D.; Trutić, N. Spectroscopic Study of Copper(II) Complexes with Carboxymethyl Dextran and Dextran Sulfate, *Russian Journal of Physical Chemistry A*, **2015**, 89(7), pp. 1254-1262, https://doi.org/10.1134/S0036024415070122

[23] Tang, H.; Dong, L.; Xia, X.; Chen, X.; Ren, M.; Shu, G.; Fu, H.; Lin, J.; Zhao, L.; Zhang, L.; Cheng, G.; Wang, X.; Zhang, W. Preparation, Optimization, and Anti-Pulmonary Infection Activity of Casein-Based Chrysin Nanoparticles, *International Journal of Nanomedicine*, **2024**, 19, pp. 5511–5522, https://doi.org/10.2147/IJN.S428045

[24] Ansari, A. A. DFT and ^{1}H NMR Molecular Spectroscopic Studies on Biologically Anti-Oxidant Active Paramagnetic Lanthanide(III)-Chrysin Complexes, *Main Group Chemistry*, 2008, **7**(1), pp. 43-56, https://doi.org/10.1080/10241220801912637

[25] Mohammadi, Z.; Sharif Zak, M.; Majdi, H.; Mostafavi, E.; Barati, M.; Lotfimehr, H.; Ghaseminasab, K.; Pazoki-Toroudi, H.; Webster, T. J.; Akbarzadeh, A. The Effect of Chrysin–Curcumin-Loaded Nanofibres on the Wound-Healing Process in Male Rats, *Artificial Cells, Nanomedicine, and Biotechnology*, **2019**, 47(1), pp. 1642-1652, https://doi.org/10.1080/21691401.2019.1594855

[26] Ng, N. T.; Abdul Keyon, A. S.; Wan Ibrahim, W. A.; Sanagi, M. M.; Sutirman, Z. A.; Mohd Marsin, F. Amino-Functionalised Chrysin as Adsorbent in Dispersive Micro-Solid Phase Extraction of Selected Heavy Metal Ions from Stingless Bee Honey, *Journal of Food Composition and Analysis*, **2023**, 123, pp. 1-12, https://doi.org/10.1016/j.jfca.2023.105561

[27] Bansal, A.; Srivastava, N.; Nagpal, K. Development and Validation of UV Spectrophotometric Method for Determination of Chrysin and Its Solubility Studies, *Journal of Applied Spectroscopy*, **2022**, 89(1), pp. 1-10, https://doi.org/10.1007/s10812-022-01338-0